Journal of Intelligent Learning Systems and Applications, 2025, 17(1), 25-35
https://www.scirp.org/journal/jilsa
ISSN Online: 2150-8410
ISSN Print: 2150-8402

Prediction of Hypersonic Aerodynamic Performance of Spherically Blunted Cone Based on Multi-Fidelity Neural Network

Jimin Chen, Guoyi He

School of Aeronautics and Astronautics, Nanchang Hangkong University, Nanchang, China
Email: hegy509@163.com

How to cite this paper: Chen, J.M. and He, G.Y. (2025) Prediction of Hypersonic Aerodynamic Performance of Spherically Blunted Cone Based on Multi-Fidelity Neural Network. *Journal of Intelligent Learning Systems and Applications*, **17**, 25-35.
https://doi.org/10.4236/jilsa.2025.171003

Received: January 8, 2025
Accepted: February 11, 2025
Published: February 14, 2025

Abstract

The rapid prediction of aerodynamic performance is critical in the conceptual and preliminary design of hypersonic vehicles. This study focused on axisymmetric body configurations commonly used in such vehicles and proposed a multi-fidelity neural network (MFNN) framework to fuse aerodynamic data of varying quality. A data-driven prediction model was constructed using a pointwise modeling method based on generating lines to input geometric features into the network. The MFNN framework combined low-fidelity and high-fidelity networks, trained on aerodynamic performance data from engineering rapid computation methods and CFD, respectively, using spherically blunted cones as examples. The results showed that the MFNN effectively integrated multi-fidelity data, achieving prediction accuracy close to CFD results in most regions, with errors under 5% in key stagnation areas. The model demonstrated strong generalization capabilities for varying cone dimensions and flight conditions. Furthermore, it significantly reduced dependence on high-fidelity data, enabling efficient aerodynamic performance predictions with limited datasets. This study provides a novel methodology for rapid aerodynamic performance prediction, offering both accuracy and efficiency, and contributes to the design of hypersonic vehicles.

Keywords

Multi-Fidelity Neural Network, Data-Driven, Spherically Blunted Cone, Axisymmetric Rotating Body, Aerothermal Modeling and Prediction

1. Introduction

Hypersonic vehicles are a global research hotspot due to their strategic military

importance. During flight, airflow through the shock wave and boundary layers decelerates and dissipates, causing temperature rises and aerodynamic heating, making heat management critical for hypersonic vehicle design. [1] [2] Aerodynamic forces and heating, collectively known as aerodynamic performance, influence layout, control, and structural design, and are fundamental for reentry vehicles such as spacecraft return capsules, space shuttles, and missiles. Traditional methods for predicting aerodynamic forces and heating include numerical simulations, experiments, and engineering approximations. The nonlinear and high-temperature effects of hypersonic flows, along with tight design schedules, further complicate predictions, highlighting the demand for more efficient methods. [3] [4] Recent advancements in data science and artificial intelligence have enabled progress in fluid dynamics. Data-driven modeling methods leverage aerodynamic data accumulated during hypersonic studies, providing new solutions to aerodynamic prediction challenges. These methods integrate various prediction approaches, achieving higher efficiency while meeting engineering requirements. [5]

Pointwise modeling (PM) is a classic data-driven aerodynamic prediction method. This approach builds prediction models for specific points of aerodynamic heating, representing the spatial distribution as scattered points over the vehicle surface, with each point modeled separately. Dreyer *et al.* [6] developed pointwise models using Kriging algorithms and 750 simulation samples to improve prediction efficiency by seven orders of magnitude compared to CFD. McNamara *et al.* [7] applied Newton's cooling law to predict convective heat transfer coefficients and adiabatic temperature distributions using limited wall temperature data. Leonard *et al.* [8] used interpolation functions to predict heating distributions for complex temperature profiles, such as those on the X-43 control surfaces. Santos *et al.* [9] applied Co-Kriging algorithms to combine multi-fidelity data, using 30 high-fidelity samples and 512 low-fidelity samples to construct aerodynamic heating models.

While these studies advanced aerodynamic heating predictions, they often focused on specific vehicle types and did not fully account for the effects of global and local geometries on aerodynamic forces and heating distributions. As a result, their scope is limited, establishing only relationships between individual aerodynamic performance metrics and input features. Li *et al.* [10] proposed SA-HFNet, a deep learning model incorporating global and local geometric features for aerodynamic heating predictions, showing good generalization. However, its preprocessing complexity risks losing shape information, and it requires extensive high-quality data for training.

This study proposes a multi-fidelity neural network-based modeling and prediction method for aerodynamic performance, enabling predictions across vehicles with similar geometries while reducing the need for extensive high-quality data. A prediction model is validated on cones of varying dimensions, demonstrating its effectiveness and generalization capabilities. Unlike previous methods, the proposed framework integrates multi-fidelity data to balance model generali-

zation and accuracy. Low-fidelity data from engineering methods provide overall trends, while high-quality CFD data correct specific details. This ensures high accuracy and efficiency, offering a practical solution for aerodynamic performance prediction in hypersonic vehicle design.

2. Prediction Model for Aerodynamic Performance of Axisymmetric Rotating Body

2.1. Pointwise Modeling Based on Generatrix

Both CFD methods and engineering rapid calculation methods require defining the primary geometric information and flight conditions of hypersonic vehicles to predict surface pressure and wall heat flux. The input features of the neural network model proposed in this paper include these two aspects, with the output being the vehicle's surface pressure and heat flux as aerodynamic performance parameters.

Flight conditions typically include freestream flow properties, vehicle attitude, and wall conditions. However, incorporating all these parameters as neural network inputs often results in overly complex network structures and requires large datasets for acceptable generalization. To simplify the model, this study selects flight altitude, freestream Mach number, and angle of attack (AOA) as input features to represent flight conditions.

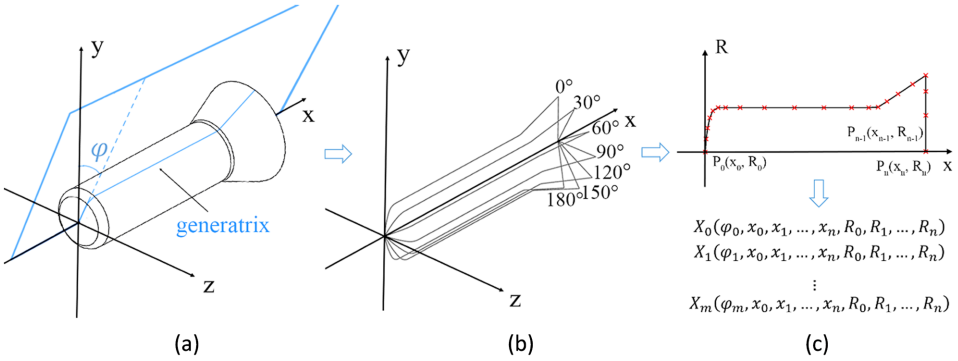

Figure 1. Vector expression method for the shape of axisymmetric body.

Vehicle geometry significantly influences surface heat flux distributions. Different shapes yield distinct aerodynamic distributions, and even within the same geometry, variations occur across surface regions. To represent geometry as input for the neural network, vectors or matrices are used, which uniquely define the geometry and allow its reconstruction. For axisymmetric bodies, a common configuration in hypersonic missiles and reentry capsules, geometry is defined by rotating a generating line around the symmetry axis. This generating line, containing most geometric information, can be represented as vectors in the x-R coordinate system. In this study, n points are non-uniformly sampled along the generating line, with higher densities in critical regions, forming vectors $(x_0, x_1, \cdots, x_n)$ and $(R_0, R_1, \cdots, R_n)$.

Additionally, m generating lines at different azimuthal angles φ are sampled (Figure 1(a) and Figure 1(b)). Each generating line is represented as a vector combining the azimuthal angle φ and the sampled x-R coordinates (Figure 1(c)). This approach simplifies predicting surface pressure and heat flux distributions by focusing on individual generating lines. Due to symmetry, predictions are only required for $\varphi = \left[0^\circ - 180^\circ\right]$. Post-processing then reconstructs the full surface distributions.

Thus, predicting the pressure and heat flux on an axisymmetric body is reduced to predicting distributions along generating lines in the x-R coordinate system for different values and flight conditions. The overall modeling and prediction process is illustrated in Figure 2.

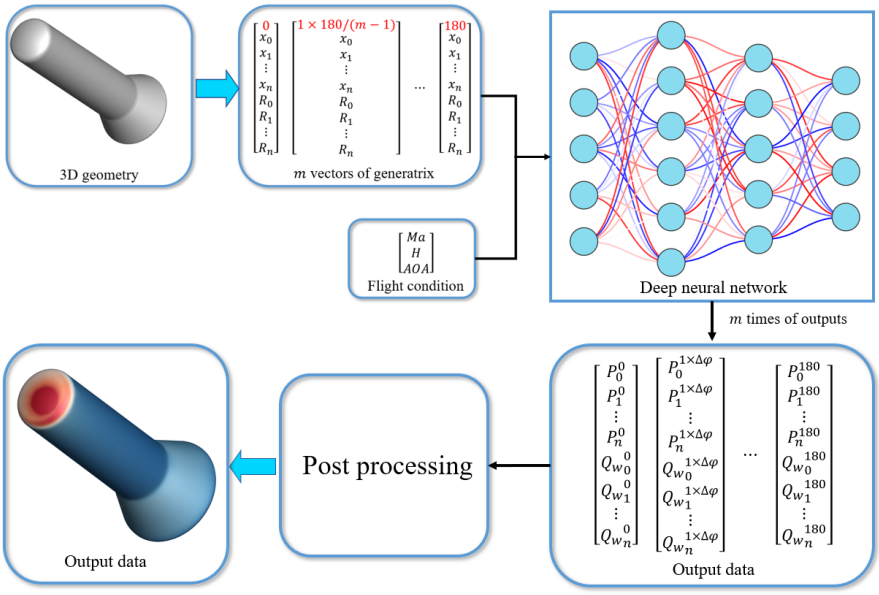

Figure 2. Modeling process of aerodynamic efficiency of axisymmetric body.

2.2. Multi-Fidelity Neural Network Architecture

Multi-fidelity neural networks (MFNNs), introduced by Meng *et al.* [11], provide a composite neural network framework capable of modeling physical systems using multi-fidelity data. Low-fidelity data are typically abundant but less accurate, while high-fidelity data are sparse and expensive. MFNNs leverage low-fidelity and high-fidelity data to enhance predictive accuracy, with high-fidelity data serving to correct the low-fidelity predictions. The relationship between high-fidelity data y_H and low-fidelity data y_L is expressed as

$$y_H = F\left(x, y_L\right), \tag{1}$$

where $F\left(.\right)$ is an unknown mapping function. Meng decomposed $F\left(.\right)$ into a linear component $F_l\left(.\right)$ and a nonlinear component $F_{nl}\left(.\right)$:

$$y_H = F_l\left(x, y_L\right) + F_{nl}\left(x, y_L\right) \tag{2}$$

The MFNN architecture based on this relationship is illustrated in Figure 3. It

consists of three fully connected neural networks: $DNN_L(x,\theta)$, which approximates the low-fidelity data y_L to capture the overall trend of y_H, and $DNN_{H1}(x,y_L,\beta_1,\gamma_1)$ and $DNN_{H2}(x,y_L,\beta_2,\gamma_2)$, which approximate $F_l(x,y_L)$ and $F_{nl}(x,y_L)$, respectively, capturing the relationship between low-fidelity and high-fidelity data. The total MFNN loss function combines the mean squared error (MSE) losses of the low-fidelity and high-fidelity networks:

$$\begin{cases} L_{MSE,MFNN} = L_{MSE,NN_L} + L_{MSE,NN_H} \\ L_{MSE,NN_L} = \dfrac{1}{N}\sum_{i=1}^{N}\left(y_{L_i} - \hat{y}_{L_i}\right)^2 \\ L_{MSE,NN_H} = \dfrac{1}{N}\sum_{i=1}^{N}\left(y_{H_i} - \hat{y}_{H_i}\right)^2 \end{cases} \tag{3}$$

Here, $\hat{y}_{L_i}$ and $\hat{y}_{H_i}$ represent the outputs of the low-fidelity and high-fidelity networks for the i-th sample.

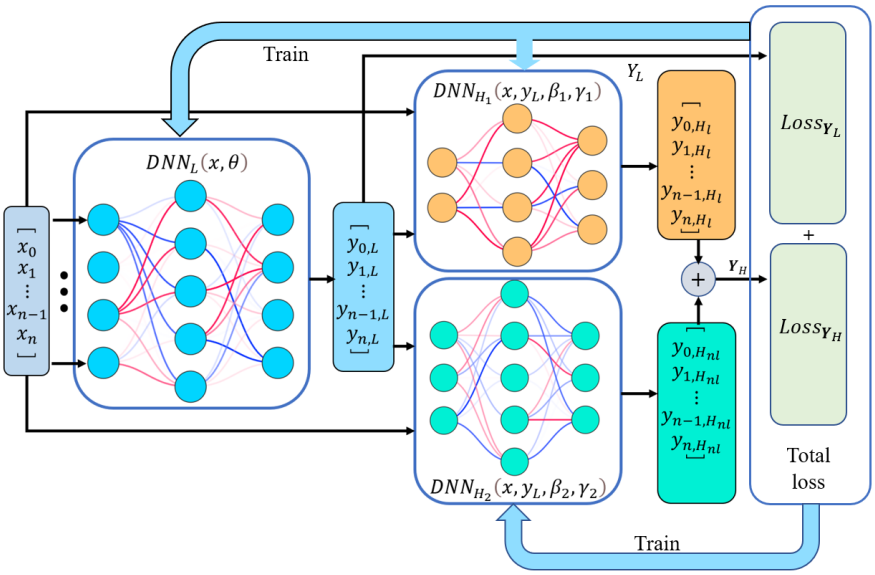

Figure 3. The structure of multi fidelity neural network.

3. Example Verification and Analysis

3.1. Construction and Preprocessing of Datasets

In this study, datasets were constructed based on the surface pressure distribution and heat flux density calculated for cones with varying geometries under different flight conditions. Additionally, the total length L of the cone, its semi-cone angle θ, and the radius R of its spherical nose satisfy the following relationship:

$$L = \left(20cos\theta - \cos^{-1}\theta + 1\right)R \tag{4}$$

This relationship allows the cone's geometry to be fully defined using only θ and R. The low-fidelity dataset was constructed using aerodynamic performance results obtained from engineering approximation. [12] The parameter ranges for

the cone's geometric dimensions and flight conditions are listed in Table 1. A full factorial design method was used to create the low-fidelity dataset. Specifically, for each cone, 19 generating lines were evenly sampled, with 62 points sampled along each line. These points, represented in the x-R coordinate system, together with flight condition parameters, and the azimuthal angle φ, formed a feature vector of size 128 for each sample. The pressure and heat flux values at the 62 points constituted a label vector of size 124. In total, the low-fidelity dataset contained 1,448,370 samples.

The high-fidelity dataset was constructed using results from a finite-volume method based on RANS (Reynolds-Averaged Navier-Stokes) simulations. The high-fidelity dataset included aerodynamic performance data for 11 cone configurations, with their geometric dimensions listed in Table 2. Each cone configuration was simulated under 25 flight conditions, which were randomly and uniformly sampled from the ranges specified in Table 1. To construct the high-fidelity dataset, 37 generating lines were uniformly sampled for each cone. The sample construction approach was consistent with that used for the low-fidelity dataset, resulting in a total of 10,175 samples.

Table 1. Range of blunt cone size parameters and flight conditions in low fidelity data.

Parameter name	Value range
Spherical nose radius (m)	{0.01, 0.02, 0.03, 0.04, 0.05, 0.06, 0.07, 0.08, 0.09, 0.1}
Semi-cone angle (deg)	{10, 11, 12, 13, 14, 15, 16, 17, 18, 19, 20}
Flight altitude (km)	{20, 25, 30, 35, 40, 45, 50}
Mach number	{5, 5.5, 6, 6.5, 7, 7.5, 8, 8.5, 9, 9.5, 10}
AOA (deg)	{0, 2.5, 5, 7.5, 10, 12.5, 15, 17.5, 20}

Table 2. Values of all blunt cone size parameters in high fidelity data.

Number	Size parameters of spherically blunted cones	
	Spherical nose radius (m)	Semi-cone angle (deg)
1	0.01	19
2	0.02	12
3	0.03	16
4	0.04	17
5	0.05	20
6	0.06	18
7	0.07	15
8	0.08	13
9	0.09	11
10	0.1	10
11	0.1	15

3.2. Prediction Results of Aerodynamic Efficiency

In this study, the Bayesian optimization method [13] was applied to optimize the

hyperparameters of the MFNN using the Optuna tuning framework. The low-fidelity dataset was divided into training and validation sets at a 4:1 ratio, while the high-fidelity dataset was divided at a 9:1 ratio. All three DNNs were trained using the Adaptive Moment Estimation (Adam) optimizer. The neural network model was constructed and trained in the PyTorch 12.4 environment on an NVIDIA GeForce RTX 4080 Super. After 943 training iterations, the low-fidelity DNN and backbone network achieved a loss of 7.987×10^{-5} on the validation set. The high-fidelity DNN reached a loss of 4.131×10^{-5} on the validation set after 1877 training iterations. Three blunt-cone configurations were selected to test the predictive performance of the MFNN. The geometric parameters of the selected blunt cones and their flight conditions are listed in Table 3. Among them, the high-fidelity training dataset included samples similar to the conditions of Case 1. In Case 2, the geometric parameters of the blunt cone were not present in the high-fidelity training or validation datasets, and in Case 3, the flight conditions were absent from the high-fidelity training and validation datasets.

Table 3. Geometric parameters and flight conditions of the blunt cones.

Case ID	Geometric parameters		Flight conditions		
	Nose Radius (m)	Semi-cone Angle(deg)	Altitude (km)	Mach Number	AOA (deg)
1	0.08	13	20	7.0	20
2	0.03	14	25	6.8	11
3	0.04	17	23	8.0	15

Based on the predictions of the trained neural network model, the surface heat flux distributions of the three test cases are shown in Figure 4, and the windward centerline heat flux is shown in Figure 5. From the figures, it can be seen that the MFNN accurately reconstructs the surface heat flux and pressure distributions of the blunt cones. In Case 1, even though the low-fidelity data (engineering approximations) exhibited large errors due to inaccurate transition position predictions, the MFNN predictions closely matched the CFD results across most regions. As shown in Figure 6(a), the windward surface error remained within 5%, demonstrating the MFNN's strong capability to fit aerodynamic heating patterns.

For Cases 2 and 3, which were not included in the training dataset, the MFNN predictions closely matched the CFD results at the blunt cone's nose stagnation region. However, in the downstream tail region, the heat flux density predictions showed significant errors. In Figure 5(b) and Figure 6(c), the windward heat flux density in the downstream tail region exhibited an upward trend, with the maximum error in Case 2 reaching an astonishing 15%. This could be attributed to the insufficient number of sampling points in the tail region when constructing input vectors with geometric features, making it challenging for the MFNN to capture the characteristics of heat flux density distribution in this area. Conversely, in the

nose region, where the number of sampling points was sufficient, the MFNN effectively learned the patterns of heat flux density distribution. In Case 3, even when the low-fidelity data (engineering approximation methods) showed a 70% error in the nose region due to inaccurate transition predictions, the MFNN predictions showed only a slight increase in error, with the maximum error remaining below 10%. Overall, the high-fidelity DNN in the MFNN demonstrated a strong corrective effect on the low-fidelity heat flux data.

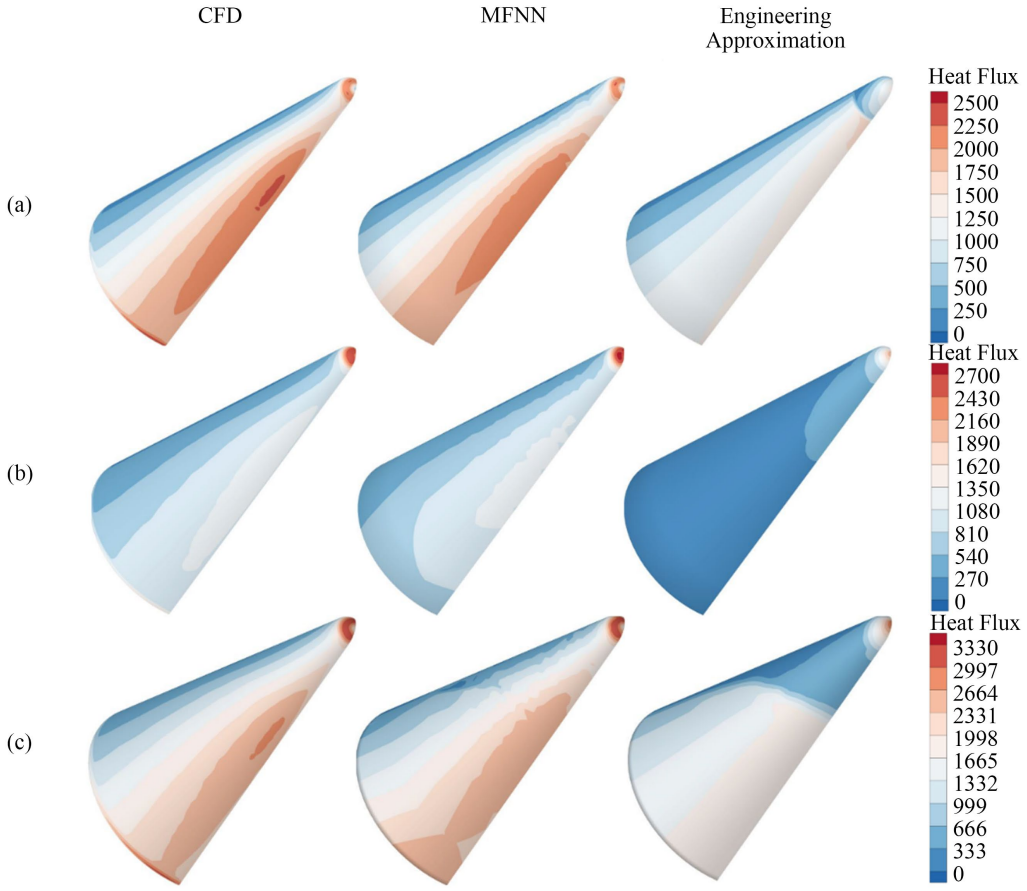

Figure 4. Surface heat flux distributions for three test cases under different prediction methods. (a) Case 1; (b) Case 2; (c) Case 3.

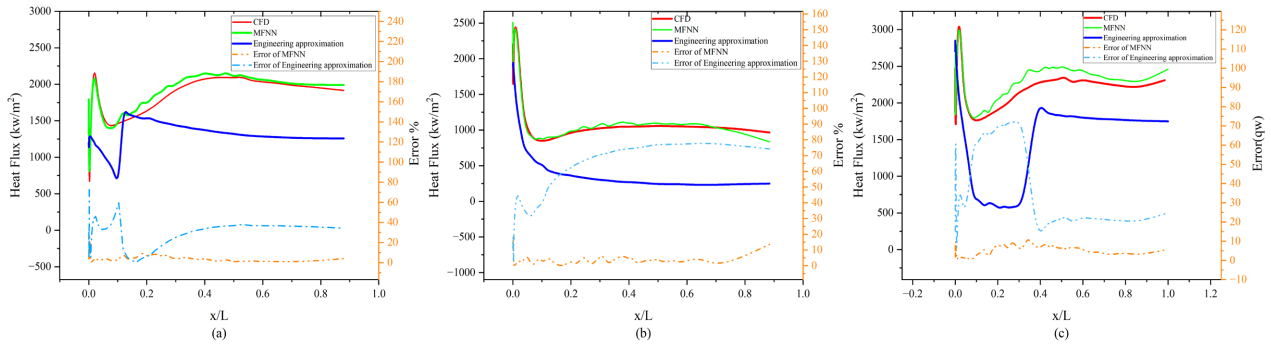

Figure 5. Heat flux at $\varphi = 180°$: (a) Case 1; (b) Case 2; (c) Case 3.

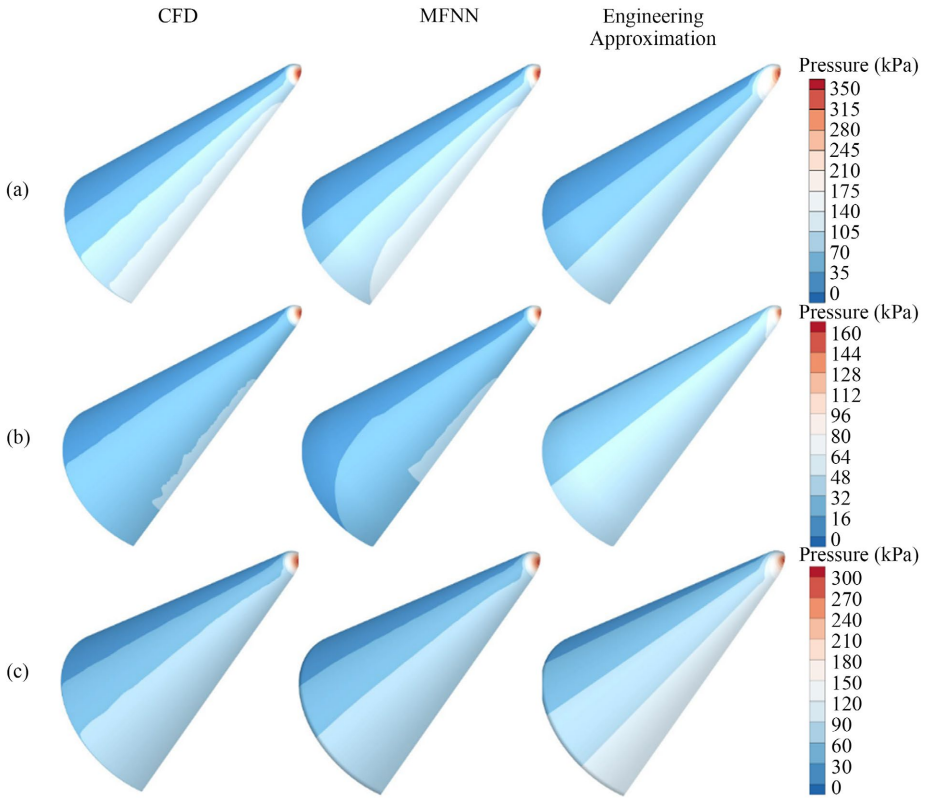

Figure 6. Surface pressure distributions for three test cases under different prediction methods. (a) Case 1; (b) Case 2; (c) Case 3.

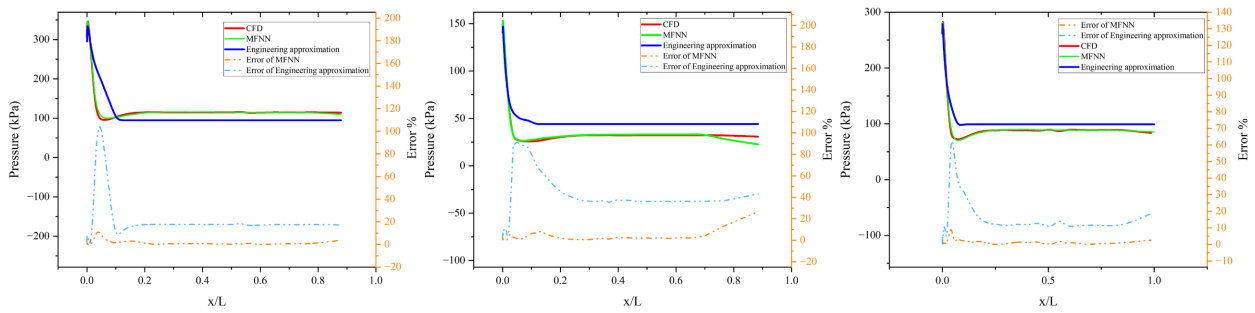

Figure 7. Pressure at $\varphi = 180^{\circ}$: (a) Case 1; (b) Case 2; (c) Case 3.

Figure 6 and Figure 7 show the surface pressure contours and windward centerline heat flux densities for the three test cases, respectively. It can be observed that the MFNN predictions for Cases 1 and 3 closely matched the CFD results, with windward heat flux densities almost overlapping and downstream errors below 3%. For Case 2, significant discrepancies were observed only in the tail region compared to the CFD results, with the windward centerline tail heat flux density error reaching 20%, likely due to insufficient sampling points in the geometric input features at this location. Additionally, Figure 7 shows that the MFNN predictions exhibited small jumps in error near the stagnation region for all three cases, with peak errors around 10%. Meanwhile, the low-fidelity data (engineering

approximations) also showed significant error jumps in this region, indicating a strong correlation between the quality of the MFNN predictions and the low-fidelity data.

Furthermore, the overall aerodynamic force prediction accuracy of the MFNN slightly outperformed its aerodynamic heating prediction accuracy. This may be attributed to the simpler patterns of aerodynamic force distributions compared to aerodynamic heating distributions, allowing the MFNN to learn aerodynamic force patterns more effectively. However, the error curves for the engineering approximation method in Figure 5 and Figure 7 indicate that the quality of the low-fidelity aerodynamic force data was better than that of the aerodynamic heating data, which might explain the higher accuracy of the MFNN's aerodynamic force predictions. In conclusion, the quality of the MFNN predictions is partially dependent on the low-fidelity data. Although the MFNN can correct the low-fidelity data to some extent, its corrective ability is limited in regions with large errors. For practical engineering applications, using higher-quality, low-fidelity data to train the MFNN could potentially improve the accuracy of its predictions.

4. Conclusions

This study addresses the rapid prediction of aerodynamic heating and proposes a multi-fidelity neural network-based modeling method for axisymmetric rotational bodies. By integrating low-fidelity data from engineering approximations and high-fidelity data from CFD, the proposed model significantly improves the accuracy of aerodynamic performance predictions. The main conclusions are as follows:

- The MFNN model exhibits excellent fitting capabilities, accurately capturing variations in aerodynamic heating and aerodynamic force distributions. Its predicted heat flux density and surface pressure distributions are largely consistent with CFD results.
- The MFNN demonstrates strong generalization capabilities, performing well under unknown flight conditions and geometric dimensions.
- Low-fidelity aerodynamic force data exhibit higher quality compared to aerodynamic heating data, resulting in better force predictions. The performance of the MFNN model partially depends on the quality of low-fidelity data, with poorer data leading to increased prediction errors.
- In regions with high sampling density, the model provides reliable predictions by effectively correcting errors through the high-fidelity network, even when low-fidelity data exhibit significant inaccuracies.

The proposed modeling and prediction method achieves high accuracy and generalization capabilities for aerodynamic heating and forces while reducing the reliance on high-fidelity data. This leads to significant advantages in computational efficiency and cost.

Acknowledgements

This work is supported by the National Natural Science Foundation of China

(grant number 12362026).

Conflicts of Interest

The authors declare no conflicts of interest regarding the publication of this paper.

References

[1] Anderson, J.D. (1989) Hypersonic and High Temperature Gas Dynamics. AIAA.

[2] Bertin, J.J. and Cummings, R.M. (2006) Critical Hypersonic Aerothermodynamic Phenomena. *Annual Review of Fluid Mechanics*, **38**, 129-157. https://doi.org/10.1146/annurev.fluid.38.050304.092041

[3] Josyula, E. (2015) Hypersonic Nonequilibrium Flows: Fundamentals and Recent Advances. American Institute of Aeronautics and Astronautics, Inc. https://doi.org/10.2514/4.103292

[4] Yuan, Z., Huang, S., Gao, X. and Liu, J. (2017) Effects of Surface-Catalysis Efficiency on Aeroheating Characteristics in Hypersonic Flow. *Journal of Aerospace Engineering*, **30**, Article ID: 04016086. https://doi.org/10.1061/(asce)as.1943-5525.0000684

[5] Kou, J. and Zhang, W. (2021) Data-Driven Modeling for Unsteady Aerodynamics and Aeroelasticity. *Progress in Aerospace Sciences*, **125**, Article ID: 100725. https://doi.org/10.1016/j.paerosci.2021.100725

[6] Dreyer, E.R., Grier, B.J., McNamara, J.J. and Orr, B.C. (2021) Rapid Steady-State Hypersonic Aerothermodynamic Loads Prediction Using Reduced Fidelity Models. *Journal of Aircraft*, **58**, 663-676. https://doi.org/10.2514/1.c035969

[7] McNamara, J.J., Friedmann, P.P., Powell, K.G., Thuruthimattam, B.J. and Bartels, R.E. (2008) Aeroelastic and Aerothermoelastic Behavior in Hypersonic Flow. *AIAA Journal*, **46**, 2591-2610. https://doi.org/10.2514/1.36711

[8] Leonard, C., Amundsen, R. and Bruce, W. (2005) Hyper-x Hot Structures Design and Comparison with Flight Data. *AIAA/CIRA 13th International Space Planes and Hypersonics Systems and Technologies Conference*, Capua, 16-20 May 2005. https://doi.org/10.2514/6.2005-3438

[9] Santos, M.J., Hosder, S. and West, T.K. (2021) Multifidelity Modeling for Efficient Aerothermal Prediction of Deployable Entry Vehicles. *Journal of Spacecraft and Rockets*, **58**, 110-123. https://doi.org/10.2514/1.a34752

[10] Li, T., Guo, L., Yang, Z., Sun, G., Zeng, L., Liu, S., et al. (2022) An Automatic Shape-Aware Method for Predicting Heat Flux of Supersonic Aircraft Based on a Deep Learning Approach. *Physics of Fluids*, **34**, Article ID: 077103. https://doi.org/10.1063/5.0098341

[11] Meng, X. and Karniadakis, G.E. (2020) A Composite Neural Network That Learns from Multi-Fidelity Data: Application to Function Approximation and Inverse PDE Problems. *Journal of Computational Physics*, **401**, Article ID: 109020. https://doi.org/10.1016/j.jcp.2019.109020

[12] Hamilton, H.H., Weilmuenster, K.J. and DeJarnette, F. (2009) Approximate Method for Computing Laminar and Turbulent Convective Heating on Hypersonic Vehicles Using Unstructured Grids. 41*st AIAA Thermophysics Conference*, San Antonio, 22-25 June 2009. https://doi.org/10.2514/6.2009-4310

[13] Snoek, J., Larochelle, H. and Adams, R.P. (2012) Practical Bayesian Optimization of Machine Learning Algorithms. arXiv: 1206.2944.